Results in Engineering 9 (2021) 100196

Contents lists available at ScienceDirect

Results in Engineering

journal homepage: www.editorialmanager.com/rineng/Default.aspx

CFD simulation of a hyperloop capsule inside a closed environment

Federico Lluesma-Rodríguez [a,b], Temoatzin González [b], Sergio Hoyas [a,*]

[a] Instituto Universitario de Matematica Pura y Aplicada, Universitat Politècnica de València, 46022, València, Spain
[b] Zeleros Global S.L. (Hyperloop), 46024, Valencia, Spain

ARTICLE INFO

Keywords:
CFD
Evacuated tube train (ETT)
Train
Vacuum tube

ABSTRACT

One of the most restrictive conditions in ground transportation is traveling through a tunnel at high speed. In those conditions waves are propagated, increasing the pressure upstream the object, and so, the drag compared to the open flow case. Although this drawback is mitigated with larger tunnels, another proposed solution is to decrease the pressure inside the tunnel. In this paper it is demonstrated that the drag coefficient is almost invariant with the pressure conditions. This effect allows, not only to have smaller tunnels with respect to the existing for standard trains, but also to enhance the speed of the train without increasing its aerodynamic losses.

1. Introduction

Electric propulsion is the future in transportation [13]. This is the reason why research in trains to overcome current speeds is performed. In that sense, aerodynamics is not a minor issue if higher velocity want to be achieved. Apart from other limits, such us the catenary contact [14] or the wheel-rail contact [2], the aerodynamics is present in the ground transportation systems as an strong limitation, specially when focusing in tunnels. Although this problem has been widely studied [4,5,7,11], this paper is focused on what occurs in a closed and controlled environment, or *Evacuated-Tube Train* (ETT).

The aim of this study is to reproduce the conditions of a train inside a closed tunnel for different blockage ratios, static pressure and speeds. To reduce the cost of the process avoiding expensive tests [12], CFD simulations have been performed. The main output is the aerodynamic drag under those conditions. The size analysed for the tunnel start from the typical one for a High-Speed Rail (blockage ratio of 0.23 [1,10]) up to 0.75.

2. Methodology

The geometry of the train is based on a model of the Transrapid Maglev train used in Ref. [3], whose maximum speed is 505 km/h [6]. The model, shown in Fig. 1, has a length of $L = 51.7$ meters and a height of $h = 3.7$ meters.

The capsule is embedded into a cylindrical fluid domain. A radial plane can be seen in Fig. 1. In order to avoid wave reflection, the inlet and outlet of the tunnel are placed 10 times away the length L of the train.

The blockage ratio β is defined as the quotient between the cross sectional area and the tunnel. Once this parameter is fixed, the height of the tunnel, h_t, is derived. The different boundaries on the domain are:

- Inlet: mass flow inlet based on train speed and reference pressure. The inlet static temperature is set to 288.15 K. Total pressure inlet is checked in results.
- Tube: moving and adiabatic wall, with the same speed as the train in a ground reference frame.
- Outlet: pressure outlet, equal to reference pressure.
- Vehicle: static and adiabatic wall.
- Axis: rotation axis to convert the 2D domain into an axilsymmetric one.

The spatial scheme used is a second order one, while the turbulence model is $k-\omega$ SST as in Ref. [3]. The solver employed is ANSYS Fluent.

The mesh is a hybrid one, formed using the blocks shown in Fig. 2. All of them are structured but two, marked with an u. These blocks are used to adapt the boundary layer mesh to the near field domain avoiding bad quality elements.

Three meshes have been proposed to perform the mesh sensibility study (see Table 1), using the drag coefficient c_D. The set up chosen for this study is the most restrictive one, having the highest speed (700 km/h), pressure (1 atm) and β (0.75). This is the case where waves are stronger, due to the larger energy on the inlet flow.

The final mesh chosen is the medium size one. The reason is because the difference in the drag with respect to the fine mesh is less than 1%, which is also lower than the difference with respect to the coarse one.

* Corresponding author.
E-mail address: serhocal@mot.upv.es (S. Hoyas).

https://doi.org/10.1016/j.rineng.2020.100196
Received 13 October 2020; Received in revised form 1 December 2020; Accepted 7 December 2020

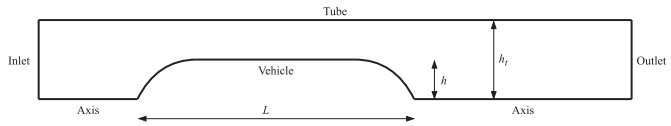

Fig. 1. Numerical domain for the case.

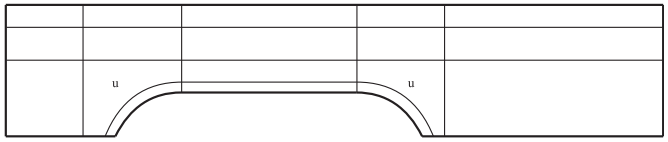

Fig. 2. Blocking chosen for the mesh.

Table 1
Meshes used in the sensibility study.

Mesh	Elements	y^+	c_D	Error [%]
Coarse	96045	4.63	16.539	–
Medium	171947	0.83	16.473	−0.40
Fine	366079	0.41	16.477	0.02

Due to wave propagation the flow is unsteady. However, to reduce the computational cost of the simulation, a comparison between a steady and an unsteady case (with time step 0.012 s) has been performed.

An unsteady Riemann solver was also tested. A priori, this solver is the one recommended for highly compressible cases, where compression waves appear. This result, along with the ones from the steady comparison, is collected in Table 2. The set up for the case is the same as for the mesh sensibility one.

Pressure based Steady solver is used for the rest of the cases, according to the results shown in Table 2. Note that the difference between this solver and the most used one (Riemann) is less than 1%, while is noticeable faster.

3. Results and conclusions

The drag coefficient is based on the wall speed, the tunnel reference pressure, and the cross sectional area of the train.

One of the uncertainties of this case is the boundary condition on the inlet and outlet. For the outlet, the pressure is fixed to the same value as the reference pressure. However, for the inlet, two different conditions have been tested:

- Impose mass flow (case 1), computed using the reference values and the area of the tunnel:

$$\dot{m} = \rho_{ref} \pi h_t^2 V_{ref}. \tag{1}$$

- Impose total pressure (case 2), computed using the reference pressure and speed:

$$p_t = p_{ref}\left(1 + \frac{\gamma - 1}{\gamma}\frac{V_{ref}^2}{\gamma R T_{ref}}\right)^{\frac{\gamma}{\gamma-1}}. \tag{2}$$

Results are shown in Table 3. Note that case 1 provides higher drag than the reference value, while case 2 is the opposite. The main reason is the larger upstream pressure when imposing the mass flow, as discussed below in Table 4.

Table 2
Different solvers used.

Solver	Drag	Error [%]
Riemann	16422718	–
Pressure based Transient	16408200	−0.088
Pressure based Steady	16407199	−0.095

Table 3
Drag for different sources or boundary conditions ($\beta = 0.5$).

V_{ref}	p_{ref}	Drag ([3])	Drag (1)	Drag (2)
700 km/h	0.022 atm	83 081 N	148 426 N	36 768 N
500 km/h	0.021 atm	44 694 N	063 446 N	13 561 N

This means that the actual value of drag is highly dependent on the upstream boundary condition. In the real case, due to wave propagation in a closed environment where more than one train is circulating, this upstream pressure varies continuously. The consequence is that the drag is not only a matter of the actual speed of the train, but also of the position of the train in the tunnel and what has happened previously, which cannot be reproduced with the presented simplification of the problem.

As a representative average result, the boundary condition chosen is mass flow. This condition is the most restrictive, and it represents the case in which all the mass flow goes through the channel between the tunnel and the train, which is more realistic in a tunnel with closed walls. This is a relevant difference with respect to an open tunnel, the one commonly studied by other authors [8,9], where leaks of mass flow can happen.

In any case, an effect that always occurs with the train traveling at this speed inside the tunnel is that it increases its pressure upstream (p_{inlet}) and decreases the speed of the flow (V_{inlet}), as seen in Table 4.

Note that, almost independently of the train speed V_{ref}, the actual flow speed upstream is similar in all cases V_{inlet}. This is a consequence of the blockage of the channel between the train and the tunnel. Regarding the pressure, imposing mass flow increases considerably the upstream pressure, a 50% at 500 km/h and a 100% at 700 km/h. When pressure is imposed, this effect also appears, but is less effective.

In any case, this increase in the inlet pressure leads to the drag differences seen in Table 3.

To further detail what occurs with the pressure, the pressure coefficient along the tunnel is represented in Fig. 3. As previously seen, there is a considerable increase in pressure on the front face of the train, larger as the tunnel gets smaller (larger β). However, the difference with the reference pressure is not remarkable.

It is important to note that downstream the train there is a strong depression, followed by an oscillatory behavior due to the obliques shock waves still present on the tunnel. Finally, there is a sudden compression of the flow to accommodate the outlet pressure. Note that for the largest tunnel ($\beta = 0.20$) there are no waves downstream, as the flow is not chocked when passing through the small gap between the train and the tunnel.

These flow patterns are better seen when representing the contours of the Mach number in Fig. 4. There, the presence of shock waves due to the high speed flow on the gap is evident.

A parametric study using different values for the velocity (500 and 700 km/h), pressure (0.01, 0.1 and 1 atm) and blockage ratio (from 0.2 to 0.75) has been performed. The results are shown in Fig. 5. There is low dependency of the drag coefficient with the pressure, which means that the drag scales linearly with that parameter. In the figure, it is also shown the big dependency with the blockage ratio. If tunnel has $\beta > 0.2$, the drag starts to grow exponentially. Remember that the common value for

Table 4
Velocity (in km/h) and pressure (in atm) for $\beta = 0.5$.

Imposed	V_{ref}	p_{ref}	V_{inlet}	p_{inlet}
Pres	700	0.022	373	0.026
Mass	700	0.022	374	0.043
Pres	500	0.021	325	0.022
Mass	500	0.021	358	0.030

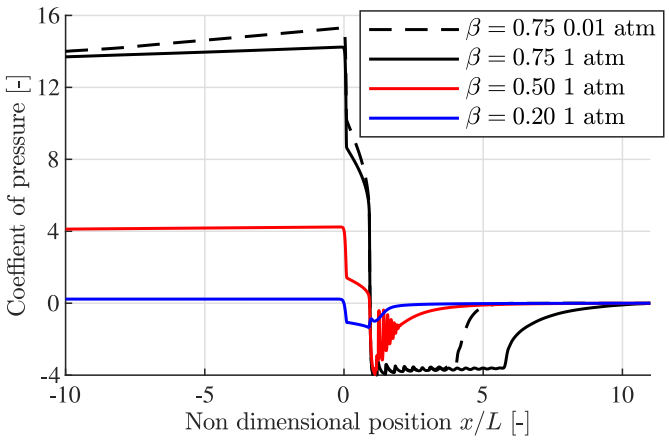

Fig. 3. Coefficient of pressure along the tube for different cases (700 km/h).

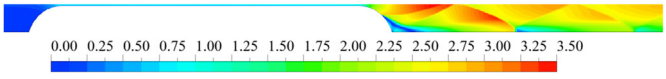

Fig. 4. Contours of Mach number for $\beta = 0.75$, 700 km/h, and 1 atm.

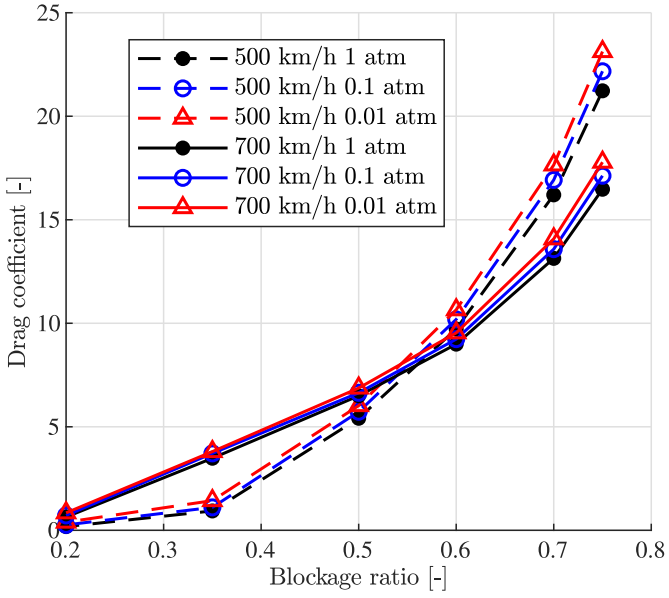

Fig. 5. Drag coefficient for the parametric study.

a High Speed Rail is 0.23, making it evident why the size of the tunnels is not smaller.

Finally, the speed affects values of the c_D curve. This is why the drag coefficient is far from being considered constant with the speed on this range.

Focusing on an example, if taken the drag of the train at 700 km/h in a common tunnel ($\beta = 0.2$), the c_D is 0.64 at atmospheric pressure. This blockage ratio means that the tunnel has a radius 124% higher than the one from the train. The same drag can be achieved when reducing the pressure to 0.1 atm and using $\beta = 0.5$ ($c_D = 6.50$), which means that the tunnel would only required to be 41% larger in terms of the radius with respect of the train.

If future ground transport want to overcome 500 km/h, a new concept where ambient pressure can be decreased must be proposed. This, allows to decrease the drag of the capsuled linearly with this parameter, leading to acceptable air resistances even at very high speeds and small tunnels.

Declaration of competing interest

The authors declare that they have no known competing financial interests or personal relationships that could have appeared to influence the work reported in this paper.

Acknowledgment

SH and FLR work have been supported by project RTI2018- 102256-B-I00 of Mineco/FEDER. FLR is partially funded buy MCIU under grant DI-17-09616.

References

[1] Adif, Tunel de Guadarrama. Technical report. Adif, URL: http://www.adifaltavelocidad.es/es_ES/infraestructuras/doc/tunelguadarrama.pdf, 2007.
[2] M. Givoni, F. Ltd, Sgm, Development and impact of the modern high-speed train: a review, Transport Rev. 26 (2006) 593–611.
[3] T.K. Kim, K.H. Kim, H.B. Kwon, Aerodynamic characteristics of a tube train, J. Wind Eng. Ind. Aerod. 99 (2011) 1187–1196, https://doi.org/10.1016/j.jweia.2011.09.001.
[4] H. Lee, C. Park, J. Lee, Improvement of thrust force properties of linear synchronous motor for an ultra-high-speed tube train, IEEE Trans. Magn. 47 (2011) 4629–4634, https://doi.org/10.1109/TMAG.2011.2158584.
[5] T. Li, X. Zhang, Y. Jiang, W. Zhang, Aerodynamic design of a subsonic evacuated tube train system, Fluid Dynam. Mater. Process. 15 (2019) 121–130, https://doi.org/10.32604/fdmp.2020.07976.
[6] Maglev Board, Transrapid Maglev shanghai, URL: https://www.maglevboard.net/en/facts/systems-overview/transrapid-maglev/transrapid-maglev-shanghai.
[7] M. Mossi, S. Sibilla, Swissmetro : Aerodynamic Drag and Wave Effects in Tunnels under Partial Vacuum, 2002.
[8] A. Orellano, Aerodynamics of High Speed Trains, 2008.
[9] R.S. Raghunathan, H.D. Kim, T. Setoguchi, Aerodynamics of high-speed railway train, Prog. Aero. Sci. 38 (2002) 469–514, https://doi.org/10.1016/S0376-0421(02)00029-5.
[10] RENFE, AVE serie 102/112, URL: https://www.renfe.com/viajeros/nuestros_trenes/aves102_ficha.html, 2020.
[11] X. Zhang, Y. Jiang, T. Li, Effect of streamlined nose length on the aerodynamic performance of a 800 km/h evacuated tube train, Fluid Dynam. Mater. Process. 15 (2019) 67–76, https://doi.org/10.32604/fdmp.2020.07776.
[12] M.S. Escarti-Guillem, S. Hoyas, L.M. García-Raffi, Rocket plume URANS simulation using OpenFOAM, Results in Engineering 4 (2019), https://doi.org/10.1016/j.rineng.2019.100056.
[13] P.K. Senecal, F. Leach, Diversity in transportation: why a mix of propulsion technologies is the way forward for the future fleet, Results in Engineering 4 (2019), https://doi.org/10.1016/j.rineng.2019.100060.
[14] F. Alkam, I. Pereira, T. Lahmer, Qualitatively-improved identified parameters of prestressed concrete catenary poles using sensitivity-based Bayesian approach, Results in Engineering 6 (2020), https://doi.org/10.1016/j.rineng.2020.100104.